

# The Mass-Metallicity-SFR Relation at $z \sim 2$ with 3D-HST

F. Cullen<sup>1\*</sup>, M. Cirasuolo<sup>2,1</sup>, R.J. McLure<sup>1</sup>, J.S. Dunlop<sup>1</sup>

<sup>1</sup>*SUPA†, Institute for Astronomy, University of Edinburgh, Royal Observatory, Edinburgh EH9 3HJ*

<sup>2</sup>*UK Astronomy Technology Centre, Science and Technology Facilities Council, Royal Observatory, Edinburgh, EH9 3HJ*

Accepted – . Received 2013 October 3

## ABSTRACT

We present new accurate measurements of the physical properties of a statistically significant sample of 103 galaxies at  $z \sim 2$  using near-infrared spectroscopy taken as part of the 3D-HST survey. We derive redshifts, metallicities and star-formation rates (SFRs) from the [OII] $\lambda$ 3727, [OIII] $\lambda$ 4958,5007 and H $\beta$  nebular emission lines in the grism spectra and exploit the multi-wavelength photometry available in the CANDELS fields to measure stellar masses. Our sample size is comparable to the current largest  $z \sim 2$  sample of galaxies with measured mass, metallicity and SFRs from Erb et al. (2006b), but our data probe lower stellar masses.

We find the mass-metallicity relation (MZR) derived from our data to have the same trend as previous determinations in the range  $0 < z < 3$ , with lower mass galaxies having lower metallicities. However, we find an offset in the relation compared to the previous determination of the  $z \sim 2$  MZR by Erb et al. (2006b), who measure metallicities using the [NII]/H $\alpha$  ratio, with our metallicities lower at a given mass. Incorporating our SFR information we find that our galaxies are offset from the Fundamental Metallicity Relation (FMR) by  $\sim 0.3$  dex. We investigate the photoionization conditions and find that our galaxies are consistent with the elevated ionization parameter previously reported in high-redshift galaxies. Using the BPT diagram we argue that, if this is the case, metallicity indicators based on [NII] and H $\alpha$  may not be consistent with the ones obtained via oxygen lines and H $\beta$ .

Using a recent determination of the theoretical evolution of the star-forming sequence in the BPT diagram we convert our measured [OIII] $\lambda$ 5007/H $\beta$  line ratios to [NII]/H $\alpha$  ratios. From the [NII]/H $\alpha$  ratio we infer systematically higher metallicities in better agreement with the FMR. We also show, using a sample of  $z \sim 2$  galaxies from Newman et al. (2013), that this trend is observed without the need to invoke theoretical conversions. Our results thus suggest the evolution of the FMR previously reported at  $z \sim 2 - 3$  may be an artifact of the differential evolution in metallicity indicators, and caution against using locally calibrated metallicity relations at high redshift which do not account for evolution in the physical conditions of star-forming regions.

**Key words:** galaxies: metallicities - galaxies: high redshift - galaxies: evolution - galaxies: star-forming

## 1 INTRODUCTION

Over recent years evidence has been accumulating for the existence of a tight relationship between mass, gas-phase metallicity (hereafter metallicity) and star-formation rate (SFR) in galaxies out to  $z \sim 2.5$ . This so called ‘fundamental metallicity relation’ (FMR) was first proposed by Mannucci et al. (2010) and Lara-Lopez et al. (2010) and has since been supported by other studies (e.g. Cresci et al. 2012;

Richard et al. 2011; Lara-López et al. 2013; Niino 2012; Belli et al. 2013). In their original paper, Mannucci et al. (2010) proposed a FMR which defines a surface in the three dimensional mass-metallicity-SFR space. Local SDSS galaxies were found to lie on the FMR surface with a residual dispersion of  $\sim 0.05$  dex in metallicity. They also found that the FMR defined locally extends out to  $z \sim 2.5$ , suggesting that the physical processes acting on star-forming galaxies have been consistent over the past  $\sim 10$  Gyr of cosmic history. Interestingly, however, they observed an evolution of 0.6 dex away from the FMR by galaxies at  $z > 2.5$ . This evolution

\* E-mail:fc@roe.ac.uk

† Scottish Universities Physics Alliance

suggests some change in the processes acting in star-forming galaxies at this epoch.

The original motivation for investigating the relationship between mass, metallicity and SFR was as an attempt to explain some of the features of the more extensively studied mass-metallicity relation (MZR). The MZR has been established across a large range in redshift from the local Universe (Tremonti et al. 2004; Liu et al. 2008; Kewley & Ellison 2008a; Panter et al. 2008), to  $z \sim 1$  (Savaglio et al. 2005; Rodrigues et al. 2008; Cowie & Barger 2008; Zahid et al. 2011; Roseboom et al. 2012),  $z \sim 2$  (Erb et al. 2006b), and out to  $z \sim 3$  (Maiolino et al. 2008; Mannucci et al. 2009). A consistent picture has emerged from these studies of a MZR similar in shape but differing in normalization out to high redshifts. At a given redshift, galaxies with lower stellar mass are found to have lower metallicities and at given stellar mass, galaxies at higher redshift are found to have lower metallicities. In the context of the FMR, the evolution of the MZR with redshift is explained as a selection effect i.e. at higher redshift galaxies are selected to have higher SFRs at a given mass and therefore lower metallicities.

An outstanding issue with the observational measurements of metallicities at high redshifts is that the only feasible method is to use strong nebular emission lines. These lines are not direct tracers of metallicity and therefore have to be calibrated in the local Universe using direct metallicity tracers such as the weak [OIII] $\lambda 4363$  auroral line, or by fitting galaxy spectra with photo-ionization models of star-forming regions where direct methods are not available (see e.g. Kewley & Dopita 2002; Nagao et al. 2006; Maiolino et al. 2008). Using these calibrations at high redshift assumes that these local-Universe calibrations sufficiently account for the change in physical conditions of star-forming galaxies with redshift. From data currently available there is evidence to suggest conditions in star-forming regions are evolving with redshift (e.g. Brinchmann et al. 2008; Hainline et al. 2009; Kewley et al. 2013a,b; Nakajima & Ouchi 2013).

One common method for studying the physical conditions in star-forming galaxies is a plot of the [NII]/H $\alpha$  vs [OIII] $\lambda 5007$ /H $\beta$  line ratios, known as a BPT diagram (Baldwin, Phillips, & Terlevich 1981). star-forming galaxies in the local Universe form a tight sequence on the BPT diagram (e.g. Kauffmann et al. 2003). However, an evolution away from this sequence is observed at high redshifts towards a higher [OIII] $\lambda 4958,5007$ /H $\beta$  ratio (e.g. Shapley et al. 2005; Erb et al. 2006b; Hainline et al. 2009; Yabe et al. 2012). At the same time an evolution in the ionization parameter of galaxies, which is a measure of the degree of excitation of HII regions, is observed, in that higher redshift galaxies are found to have higher ionization parameters (e.g. Lilly et al. 2003; Hainline et al. 2009; Richard et al. 2011; Nakajima et al. 2013). This evolution toward higher ionization parameters has been used to explain the offset of high redshift galaxies from the local Universe relation on the BPT diagram (e.g. Brinchmann et al. 2008; Kewley et al. 2013a,b). Most recently Nakajima & Ouchi (2013) suggest that the apparent evolution of galaxies away from the FMR at  $z \sim 3$  can be explained if the evolution of ionization parameter is accounted for. Interestingly, using a sample of low-redshift analogs of  $z > 1$  galaxies and measuring metallicities directly with [OIII] $\lambda 4363$ , Ly et al. (2013) observe an offset from the FMR of the order 0.1 - 1 dex similar to that observed at  $z$

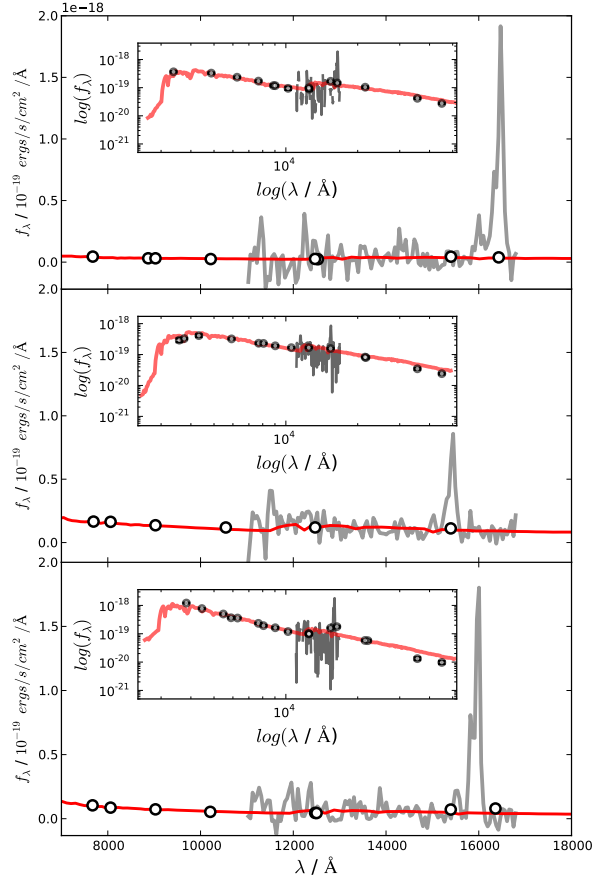


**Figure 1.** The continuum fits to three galaxies in our sample. Each panel shows a grism spectra in the rest frame with the continuum fit from the SED plotted in red and the photometry points as black empty circles. Inset in each panel is the full best-fitting SED of the galaxy with the photometry and grism spectra over plotted.

$\sim 3$ . Current observational evidence seems to suggest that the changes in physical conditions of star-forming regions is affecting metallicity measurements.

In this paper we aim to provide additional observational constraints on the MZR and FMR at  $z \sim 2$ , using a sample of star-forming galaxies selected from the 3D-HST near-IR spectroscopic dataset. 3D-HST (Brammer et al. 2012) is a slitless spectroscopic survey with the Wide-Field Camera 3 (WFC3) on the Hubble Space Telescope (HST) and provides an ideal dataset for obtaining a large sample of  $z \sim 2$  galaxies for which metallicities can be measured, as the [OII] $\lambda 3727$ , H $\beta$  and [OIII] $\lambda 4958,5007$  nebular emission lines commonly used for metallicity measurements fall into the grism spectra in the redshift range  $2 < z < 2.3$ . We provide, for the first time, a sample of galaxies similar in size to the current largest dataset of  $z \sim 2$  galaxies with measured metallicities studied by Erb et al. (2006b). Since the Erb et al. (2006b) study was based on a sample of UV-selected star-forming galaxies observed from the ground, our line-flux limited sample taken with the HST allows us to probe lower SFRs than the Erb et al. (2006b) data. Finally, since Erb et al. (2006b) measure metallicities with the H $\alpha$  and [NII] nebular lines, we are able to use an independent method with the [OII] $\lambda 3727$ , H $\beta$  and

[OIII] $\lambda$ 4958,5007 lines. These are the same nebular emission lines used for measuring metallicities in the  $z \sim 3$  studies (Maiolino et al. 2008; Mannucci et al. 2009), and therefore our data provide useful insight into the observed shift of the FMR between  $z \sim 2$  and  $z \sim 3$ .

The paper is organised as follows: in Section 2 we describe the spectroscopic and photometric data, and the measurement of stellar mass, star-formation rates and metallicities from these data. In Section 3 we describe the results of this paper in the context of the MZR, FMR and photoionization conditions of the galaxies in our sample. We compare our results to those from previous  $z \sim 2$  studies and summarize our results in Section 4. Throughout we assume a cosmology with  $\Omega_m = 0.3$ ,  $\Omega_\Lambda = 0.7$ , and  $H_0 = 70 \text{ km s}^{-1} \text{ Mpc}^{-1}$ .

## 2 THE DATA

In this paper we take advantage of two complimentary datasets: a spectroscopic sample drawn from the 3D-HST spectroscopic survey (Brammer et al. 2012) and photometric data taken as part of the CANDELS survey (Grogin et al. 2011; Koekemoer et al. 2011). The combination of these data allows us to calculate the required physical properties for the galaxies in our sample.

### 2.1 3D-HST Spectroscopic Data

The spectroscopic data used in this paper are part of the 3D-HST observations described in Brammer et al. (2012). The 3D-HST survey provides low resolution ( $R \sim 130$ ) spatially resolved near-IR grism spectra over the wavelength range  $1.1 - 1.68 \mu\text{m}$  taken with the WFC3 G141 grism on the *Hubble Space Telescope* (HST). The survey covers  $675 \text{ arcmin}^2$  providing spectroscopic follow-up of three quarters of the deep near-IR CANDELS imaging in 5 fields (AEGIS, COSMOS, GOODS-S, GOODS-N and UDS).

A modified version of the publicly available pipeline described in Brammer et al. (2012) was used to reduce the 3D-HST grism exposures utilising the AXE software package (Kümmel et al. 2009). Objects are selected from a CANDELS F160W ( $H_{160}$ ) mosaic of the given field down to a limiting magnitude of  $H_{160} = 26$  (AB mag). The 4 raw direct images of the 3D-HST pointing are combined using the IRAF task MULTIDRIZZLE and positional offset from the CANDELS mosaic are calculated using TWEAKSHIFTS. The 4 raw grism images are combined using MULTIDRIZZLE and aligned to the reference mosaic using the shifts calculated on the direct image. The standard set of AXE tasks are then used to fully reduce the grism pointings to individual 1D and 2D spectra. A custom method for estimating background subtraction as described in Brammer et al. (2012) is implemented, this takes into account the variation of IR background across the sky which cannot be fully accounted for in default grism master sky background (Kümmel et al. 2009).

We carefully treat the contamination of the grism spectra. With grism spectroscopy any given spectrum can be contaminated by the spectra of nearby sources. To mitigate this effect, in some grism surveys, exposures are taken at different position angles in the hope that multiple dispersion directions reduce the chances of a spectrum being severely

contaminated (e.g Pirzkal et al. 2013). However, grism exposures in the 3D-HST survey are taken at only one position angle, and so a reliable quantitative estimation of spectral contamination is required. We estimate the contamination by using the images in the F850LP, F125W and F160W bands available in the CANDELS fields. We use the AXE task FCUBEPREP to construct model grism images using the photometric and morphological properties derived from the images; the mosaics are extended around the field of view (FOV) of the grism exposure to account for sources outside the FOV whose spectra are dispersed onto the grism image.

#### 2.1.1 Redshift determination

Due to the low resolution of the grism spectra, care must be taken when deriving galaxy redshifts. In many cases only one emission line is visible in the spectrum and so combining spectral redshift information with photometric redshift estimates is required. We estimate redshifts using a combination of spectral template fitting and photometric redshifts. For spectral fitting we use galaxy templates from the K20 survey (Mignoli et al. 2005), binned to the resolution of the grism spectra and calculate probability distributions derived from a  $\chi^2$  fit. The redshift probability distribution from spectra fitting is then combined with a photometric redshift probability distributions calculated from the broad band photometry of the galaxies using the EAZY code (Brammer et al. 2008).

#### 2.1.2 Final spectroscopic sample

The sample used in this paper is drawn from 3 of the 5 fields covered by 3D-HST: GOODS-S, COSMOS and UDS fields. Within the grism wavelength range the prominent [OII] $\lambda$ 3727,  $H\beta$  and [OIII] $\lambda$ 4958,5007 emission lines are observable at  $2.0 < z < 2.3$ . These emission lines can be used for estimating SFRs and metallicities of galaxies as described in Maiolino et al. (2008) and also allow accurate redshift determination. The final sample contains 103 galaxies. 96/103 galaxies are line-flux selected from the 3D-HST data down to a flux limit in [OIII] $\lambda$ 5007 of  $5 \times 10^{-18} \text{ ergs/cm}^2/\text{s}$ . All 3D-HST selected galaxies have been visually inspected to ensure quality and reliable contamination estimates. 7/103 galaxies have been selected from a spectroscopic catalogue in GOODS-S. Only spectra with high-quality redshift flags in good agreement with our photometric redshifts, or those whose spectroscopic redshift is in disagreement with our photometric redshift but whose grism spectra on inspection show clear emission line signatures which our automatic fitting procedure has missed, are selected. Our final catalogue was matched to the Chandra 4MS X-ray catalog in GOODS-S (Xue et al. 2011) and Chandra 1.8Ms X-ray catalog in COSMOS (Civano et al. 2012) to remove AGN from the sample; 3 galaxies were removed leaving 100 galaxies on which the analysis described below was performed.

### 2.2 CANDELS Photometric Data

The photometric data are taken from three separate catalogues for the GOODS-S, UDS and COSMOS fields. All photometry covers the rest-frame UV to mid-infrared

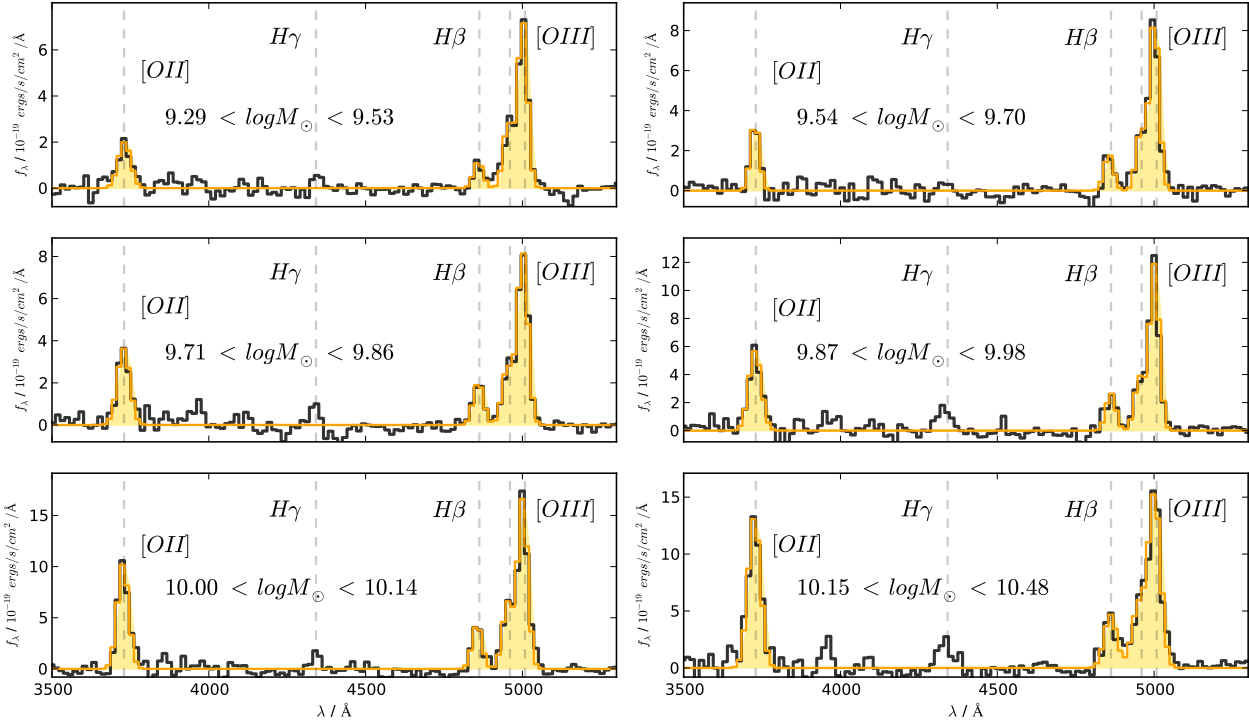


**Figure 2.** Rest-frame stacked spectra of galaxies in our sample split into six bins of increasing stellar mass. Each panel is labeled with the range of stellar mass in each bin and the [OII] $\lambda$ 3727, H $\beta$  and blended [OIII] $\lambda$ 4958,5007 emission lines are marked by dashed lines. The stacked spectra are shown in black with the fit to the emission lines overlaid in orange. The fitting procedure is described in section 2.3.2. Also indicated is the H $\gamma$  line which begins to show up in the high-mass stacks.

(Spitzer/IRAC 3.6 and  $4.5\mu\text{m}$ ). In both GOODS-S and UDS we take the photometry from existing CANDELS catalogues described in Guo et al. (2013) and Galametz et al. (2013) respectively. For COSMOS we produce a new catalog by first convolving all the available optical and mid-infrared imaging to a common PSF ( $0.8''$ ) and performing aperture photometry using F160W as the detection band (see Bowler et al. (2012) for details). The Spitzer/IRAC 3.6 and  $4.5\mu\text{m}$  photometry is added by directly fitting the IRAC images using  $K$ -band positions and shape information from UltraVISTA (McCracken et al. 2012).

### 2.2.1 Stellar masses and SFRs from SED fitting

Stellar masses and SFRs for individual galaxies are estimated from SED fitting using the publicly available code LEPAHRE (Ilbert et al. 2006). We run LEPAHRE with solar-metallicity Bruzual & Charlot (2003) templates assuming  $\tau$  model star-formation histories with  $\tau = 0.3, 1, 2, 3, 5, 10, 15, 30$  Gyr. The Calzetti et al. (2000) attenuation law is used to account for dust extinction with  $E(B - V)$  values ranging from 0 to 0.6. The age of the model is allowed to vary between 0.05 Gyr and the age of the Universe at the spectroscopic redshift of the galaxy. The normalization factor required to scale the best-fitting template to the observed magnitudes in each band gives the stellar mass and the SFR is estimated from the rest frame UV magnitude corrected for the best-fitting dust extinction.

## 2.3 Galaxy Metallicities and SFRs from Spectra

### 2.3.1 Galaxy stacking procedure

We measure spectral properties (SFR and metallicity) for all the individual galaxies. However, due to the low S/N of some of the spectra we also stacked the spectra in bins of stellar mass, following the method of Erb et al. (2006b). The mass bins were chosen such that each bin contained a similar number of galaxies. Each individual spectrum was shifted to the rest frame and the continuum of each galaxy was subtracted by interpolating the best-fitting BC03 model SED onto the same wavelength grid and normalizing to the galaxy spectra with the emission lines masked. Examples of continuum fits to galaxies are shown in Fig. 1. This method of continuum subtraction was preferred to fitting a simple low order polynomial to the galaxy spectra as the SED model can better fit the  $4000\text{\AA}$  break crossing the [OII] $\lambda$ 3727 emission line and also accounts for the underlying H $\beta$  absorption in the stellar continuum. Within each mass bin the galaxy spectra were interpolated to a common wavelength grid and we determine the median flux within each wavelength bin. The final stacked galaxy spectra are shown in Fig. 2. For consistency we have checked that removing the continuum from each galaxy individually before stacking, and removing a stack of SED models from a stack of the observed galaxy spectra does not change our results. All quantities described below were measured for both the individual spectra and the stacks.

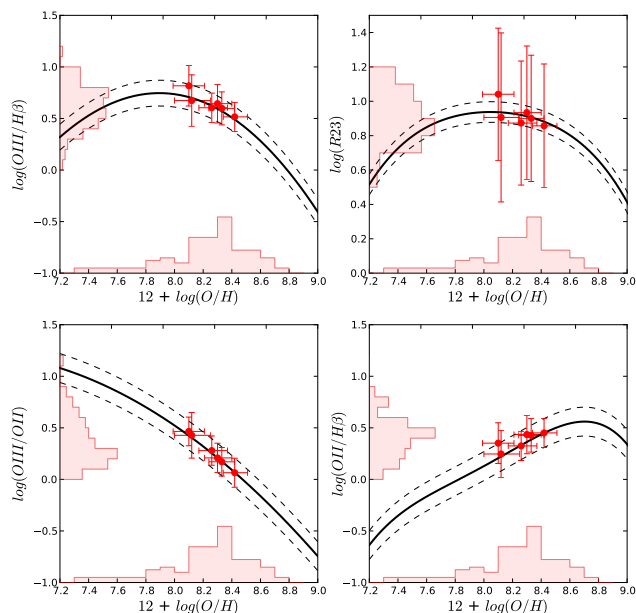


**Figure 3.** Relationship between line ratio and derived metallicity values for each of the four metallicity calibrations used to determine galaxy metallicities in this paper. The calibration curves are taken from Maiolino et al. (2008). Shown as red solid circles are the metallicities derived using a combination of all four line ratios as described in Sec. 2.3.3. The red histograms represent the distributions of individual galaxies in the sample.

### 2.3.2 Line fluxes

We measured line fluxes from the continuum-subtracted grism spectra in the following way. For the [OIII]λ4958,5007 doublet and Hβ lines we fit a triple gaussian allowing the height of each gaussian to vary. Since the [OIII]λ5007 line always has the highest S/N we fit the centroid of the [OIII]λ5007 line and fix the centroids of [OIII]λ4958 and Hβ given the best-fitting [OIII]λ5007 centroid and redshift. We allow the fit to vary the width of the [OIII]λ5007 line; the width of the [OIII]λ4958 and Hβ lines are fixed to the best-fitting width of the [OIII]λ5007 line. The [OIII]λ4958,5007 lines are blended due to the low resolution of the grism spectra, and so to measure the flux in these lines we used two methods. First we fit two gaussians and use the best-fitting parameters for each line directly from the fit, secondly we sum the two gaussians from the best-fitting and take the [OIII]λ5007 flux to be 3/4 of the total (Storey & Zeppen 2000), this follows previous methods for measuring the [OIII]λ4958,5007 line fluxes from grism spectra (Trump et al. 2013). We have checked that both methods are fully consistent and do not affect the results of this paper. For the [OII]λ3727 line we fitted a single gaussian allowing the centroid, line-width and height to vary. Examples of the line fits to the stacked spectra are shown in Fig. 2.

### 2.3.3 Gas phase metallicity

The gas-phase metallicity of a galaxy is a measure of the abundance of metals relative to hydrogen in the ISM and is most commonly quoted in terms of the oxygen abundance ratio  $12 + \log(\text{O}/\text{H})$ . Measuring the metallicity at high red-

shifts relies on using ratios of various strong, optical emission lines emanating from HII regions, therefore tracing the gas around newly-formed stars. These line ratios are a combination of strong hydrogen recombination lines such as Hα and Hβ, and collisionally excited forbidden transitions in metals such as [NII], [OII]λ3727 and [OIII]λ4958,5007.

Unfortunately the ratios of the strengths of these lines do not depend solely on the element abundances but have other dependences (e.g. gas density, hardness of ionizing radiation, etc.), and therefore must be calibrated against direct metallicity tracers. At low metallicities, in the local Universe, the electron temperature  $T_e$  method (Pettini & Pagel 2004) can be used to calibrate the nebular lines. At higher metallicities the electron temperature methods cannot be used and we rely on photoionization modeling of HII regions (Kewley & Dopita 2002). Various attempts have been made to calibrate these strong nebular line ratios across a wide range of metallicity values (e.g. Nagao et al. 2006; Kewley & Ellison 2008b; Maiolino et al. 2008). These authors give various recipes for calculating the gas phase metallicity of a galaxy from line ratios of optical emission lines. It is important to note that inferred values of metallicities depend crucially on the calibration adopted, and therefore when making comparisons all results must be converted to a consistent calibration (Kewley & Ellison 2008a). In this paper we use the calibrations described in Maiolino et al. (2008), we choose this calibration as it was also used in the original investigation of the FMR (Mannucci et al. 2010).

We measure metallicities using the [OII]λ3727, [OIII]λ4958, [OIII]λ5007 and Hβ emissions lines via a method similar to that used for the  $z \sim 3$  galaxies in the AMAZE and LSD surveys (Maiolino et al. 2008; Mannucci et al. 2009). However, in contrast to these studies, we do not fit to metallicity and extinction simultaneously across all line ratios. However, both Maiolino et al. (2008) and Mannucci et al. (2009) note that their fit, whilst constraining the metallicity, does not simultaneously provide good constraints on the dust extinction, implying the derived metallicity is weakly dependent on the value of dust extinction adopted. We use the best-fitting  $A_v$  returned from SED fitting and de-redden the spectra according the Calzetti et al. (2000) prescriptions. We measure all line ratios available which have metallicity calibrations given in Maiolino et al. (2008) (Figure 5 in their paper). Specifically the line ratios are  $R_{23} (= [\text{OII}]\lambda 3727 + [\text{OIII}]\lambda 4958 + [\text{OIII}]\lambda 5007 / \text{H}\beta)$ ,  $[\text{OIII}]\lambda 5007 / \text{H}\beta$ ,  $[\text{OIII}]\lambda 5007 / [\text{OII}]\lambda 3727$  and  $[\text{OII}]\lambda 3727 / \text{H}\beta$ . The line ratios and calibration curves are shown in Fig. 3.

To measure a metallicity for a galaxy stack we first calculate the observed line ratio in each of the four diagrams. At each value of metallicity, within a large range ( $5 < \log(\text{O}/\text{H}) + 12 < 10$ ), we calculate, for each calibration curve, a  $\chi^2$  statistic from the difference between the observed line ratio and calibration line ratio at that metallicity. Thus for all four calibration curves we construct a  $\chi^2$  vs  $\log(\text{O}/\text{H}) + 12$ . We combine the  $\chi^2$  values from each of the four diagrams to construct an overall  $\chi^2$  vs  $\log(\text{O}/\text{H}) + 12$ . We take the metallicity at the minimum of the combined  $\chi^2$  as the best-fitting metallicity. We take the  $1\sigma$  confidence intervals to be within  $\Delta\chi^2 = 1$  of the best-fitting value.

To check for consistency we take the line ratios from the Maiolino et al. (2008) and Mannucci et al. (2009) papers,



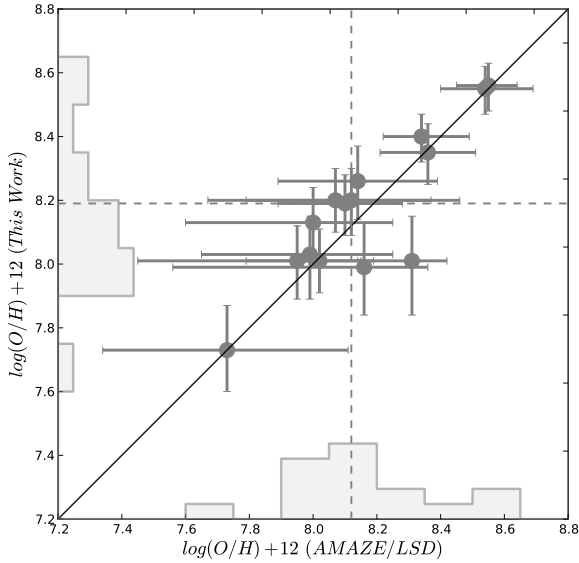


**Figure 4.** Comparison of our measurement of metallicity for the  $z \sim 3$  galaxies in Maiolino et al. (2008) and Mannucci et al. (2009) compared to the metallicities quoted in those papers. The mean and median offset of the measured metallicities are 0.013 and 0.004 dex respectively. On each axis the histograms represent the distribution of the individual points and the dashed lines represent the median of those distributions.

de-redden via the best-fitting extinctions quoted, and measure the metallicities in the same way as described above. We compare these measured metallicities to the metallicities quoted in those papers. Fig. 4 shows the results of this test; our method agrees very well across the all 15 data points with median and average difference of 0.004 and 0.013 dex respectively.

#### 2.3.4 star-formation rates

We measure star-formation rates from the  $H\beta$  line flux, first converting to luminosity and then using the common conversion factor  $H\alpha/H\beta = 2.86$  (Kennicutt 1998). We then scale down by a factor 1.7 to convert to a Chabrier (2003) IMF. Use of the  $H\alpha/H\beta$  conversion factor relies on the assumption that the galaxies in the stacks have  $E(B - V) = 0$  after the de-reddening of individual spectra, therefore a good estimate of the extinction suffered by emission lines in the galaxy is required. There has been much debate in the literature as to whether the extinction returned from SED fitting, which corresponds to the extinction in the stellar continuum, is the same as the extinction suffered by emission lines. Emission lines emanate from dusty star-forming regions and therefore could potentially suffer larger extinction than stars. Calzetti et al. (2000) find that  $E(B - V)_{stars} = (0.44 \pm 0.03)E(B - V)_{gas}$  for local starburst galaxies and similar corrections have been reported for galaxies out to  $z \sim 2$  (e.g. Förster Schreiber et al. 2009; Cresci et al. 2012; Yabe et al. 2012). However other  $z \sim 2$  studies find, when comparing SFRs derived from line fluxes to SFRs derived from SED

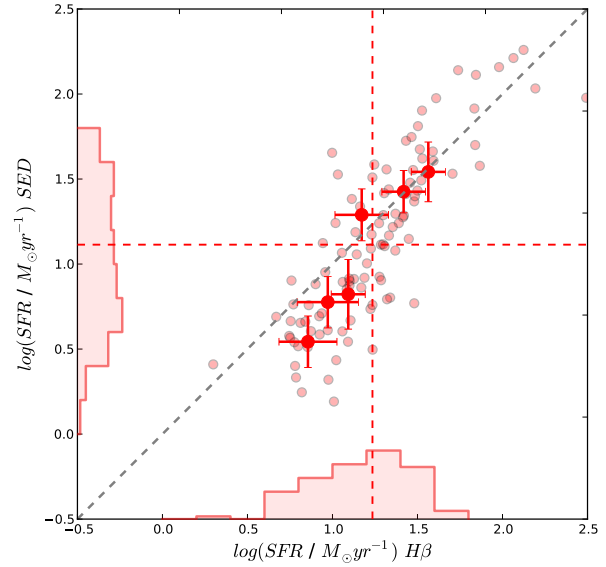


**Figure 5.** A comparison of SFR measured from the  $H\beta$  line with SFR as derived from SED fitting. The galaxy stacks are shown as the large red points with error bars. The SED SFRs for the stacks are taken as the median of the SED-derived SFRs of individual galaxies within the stack. The small red points represent the individual galaxies. On both axes histograms of the values for the individual galaxies are plotted and the dotted red lines show the median values for each distribution. The  $H\beta$  and SED methods are in good agreement. Respectively, the median and median absolute deviation (MAD) of the SFRs of the whole galaxy sample are  $17.2 \pm 8.8 M_{\odot} \text{yr}^{-1}$  and  $13.0 \pm 12.3 M_{\odot} \text{yr}^{-1}$ .

fitting, that  $E(B - V)_{stars} \sim E(B - V)_{gas}$  (e.g. Erb et al. 2006a; Hainline et al. 2009).

To get a sense as to whether we are making sensible dust corrections we can compare our best-fitting SFR from SED fitting to that derived from the de-reddened line flux. The comparison is shown in Fig. 5. The figure shows that the two independent measures of SFR are in good agreement for the galaxy stacks, for the  $H\beta$  and SED methods respectively the median and median absolute deviation (MAD) of the SFRs of the whole galaxy sample are  $17.2 \pm 8.8 M_{\odot} \text{yr}^{-1}$  and  $13.0 \pm 12.3 M_{\odot} \text{yr}^{-1}$ . Given the good agreement between the SFRs we adopt the  $E(B - V)$  values returned by SED fitting for correcting the emission lines therefore supporting the previous results at  $z \sim 2$  claiming that  $E(B - V)_{stars} \sim E(B - V)_{gas}$ .

### 3 RESULTS: MZR AND FMR

In this section we present the results of our study of the MZR and FMR, exploring the position of the 3D-HST  $z \sim 2$  emission line galaxies in the MZ plane and on the FMR surface. Throughout we compare to the previous  $z \sim 2$  sample of Erb et al. (2006b) as it represents the largest single sample of  $z \sim 2$  galaxy metallicities to date, and directly follows our method of stacking low S/N galaxies into bins of stellar mass.

### 3.1 Mass-Metallicity Relation

Fig. 6 shows the MZR for our data compared to the MZR from Erb et al. (2006b). Erb et al. (2006b) measured metallicities from the  $[\text{NII}]/\text{H}\alpha$  ratio using the calibration of Pettini & Pagel (2004), so we convert their data to the Maiolino et al. (2008) calibration to keep the metallicity scales consistent. It is important that strong line metallicity diagnostics are compared using the same calibration since it has been noted that mismatches between different calibration scales can cause systematic offsets in derived metallicities (e.g. Kewley & Ellison 2008b). Erb et al. (2006b) used a Chabrier IMF to derive stellar masses so no mass conversion is necessary for consistency with our analysis. As a cross check we have run the photometric data from their paper through LEPHARE and confirmed we derive similar stellar masses.

Our data support the existence of the MZR at  $z \sim 2$ . It can be seen from Fig. 6 that we find, in agreement with many other studies of the MZR, a decrease in metallicity with decreasing stellar mass. Across the range of stellar mass  $9.3 < \log(M/M_\odot) < 10.5$  we observe a decrease of  $\sim 0.3$  dex in metallicity. Our data extends the Erb et al. (2006b) study as we probe masses below  $\log(M/M_\odot) \sim 10.0$  where their data could only place an upper limit on the metallicity. However at a given value of stellar mass we measure lower metallicities than Erb et al. (2006b). This discrepancy is of the order  $\sim 0.3$  dex in the highest mass bins. Below we explore a possible explanation for this offset given by the FMR.

### 3.2 Fundamental Metallicity Relation

To investigate the FMR the SFR of the galaxy stacks were measured from the  $\text{H}\beta$  line flux as described in Sec. 2.3.4. We have also checked that our results remain unchanged if we instead take, as the  $\text{H}\beta$  flux of the stacks, the median  $\text{H}\beta$  flux of the individual galaxies with the stack. The FMR equation as described in Mannucci et al. (2010) is given by:

$$12 + \log(O/H) = 8.90 + 0.37m - 0.14s - 0.19m^2 + 0.12ms - 0.054s^2 \quad (1)$$

where  $m = \log(M/M_\odot) - 10$  and  $s = \log(\text{SFR})$  in solar units.

With this equation it is possible to predict the metallicity of a galaxy if the mass and SFR are known. According to the FMR, measuring lower metallicity in a given stellar mass bin should indicate that the average SFR in that bin is higher. Therefore given we measure lower metallicities than Erb et al. (2006b) across our stellar mass bins (Fig. 6), we should also observe elevated average SFRs in those bins. However as illustrated in Fig. 7 the average SFR within our stellar mass bins is lower than the Erb et al. (2006b) data, converging to similar values towards the higher mass bins in our sample ( $\sim 10^{10} M_\odot$ ). This implies at least one of these data sets is in contradiction to the FMR. The problem is not alleviated by taking our SFRs from SED fitting as these are on average slightly lower than the  $\text{H}\beta$  derived SFRs as discussed in Sec. 2.3.4.

In Fig. 6 the solid light-red and grey lines represent the predicted positions of the galaxy stacks for our data and Erb et al. (2006b) respectively on the M-Z plane given the measured SFRs plotted in Fig. 7. The solid lines in Fig. 7 are

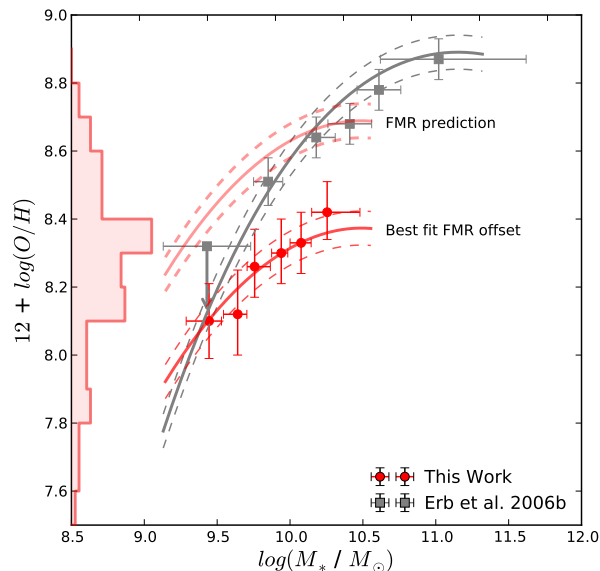


**Figure 6.** The mass-metallicity relationship for  $z \sim 2$  galaxies. Red circles represent the galaxy stacks presented in this paper with metallicities derived from the  $[\text{OII}]\lambda 3727$ ,  $[\text{OIII}]\lambda 4958, 5007$  and  $\text{H}\beta$  nebular emission lines. The red histogram shows the distribution of metallicities for the individual galaxies in the stacks. A decrease in metallicity with decreasing stellar mass is observed consistent with the general form of the MZ relation up to  $z \sim 3$ . The grey squares represent the  $z \sim 2$  MZ relation from Erb et al. (2006b) with metallicities derived from  $[\text{NII}]$  and  $\text{H}\alpha$ . The top light-red solid line represents the FMR prediction for the position of the galaxies in this paper on the MZ plane (see Sec. 3.2 for details). A significant offset of  $\sim -0.3$  dex in metallicity is observed between the FMR prediction and the measured metallicities. The form of the FMR given this offset is shown in the bottom dark-red solid line. The solid grey line represents the FMR prediction for the position of the Erb et al. (2006b) galaxies in the MZ plane with  $\pm 1\sigma$  error bars. The Erb et al. (2006b) data is in good agreement with the FMR prediction as previously noted by Mannucci et al. (2010). This reason for this discrepancy in the  $z \sim 2$  data, as argued in the text, is due to the different nebular emission lines being used to derive metallicities.

$2^{\text{nd}}$  order polynomial fits through the points in the M-SFR plane; we input these into Eq. 1 to derive the predicted M-Z plane positions. It can be seen that the Erb et al. (2006b) data are in good agreement with the FMR prediction as has been previously noted in Mannucci et al. (2010). However, our data are significantly offset to lower metallicities than predicted from the FMR. Fixing the form of Eq. 1 but varying the normalization gives a best-fitting equation to our data of:

$$12 + \log(O/H) = 8.57 + 0.37m - 0.14s - 0.19m^2 + 0.12ms - 0.054s^2 \quad (2)$$

equating to a  $\sim 0.3$  dex offset in metallicity. This line is also plotted in Fig. 6 as a solid dark-red line.

The offset is illustrated more quantitatively in Fig. 8. This figure shows the difference between metallicity observed and the metallicity predicted from the FMR given the  $\text{H}\beta$  derived SFR and the median values of stellar mass

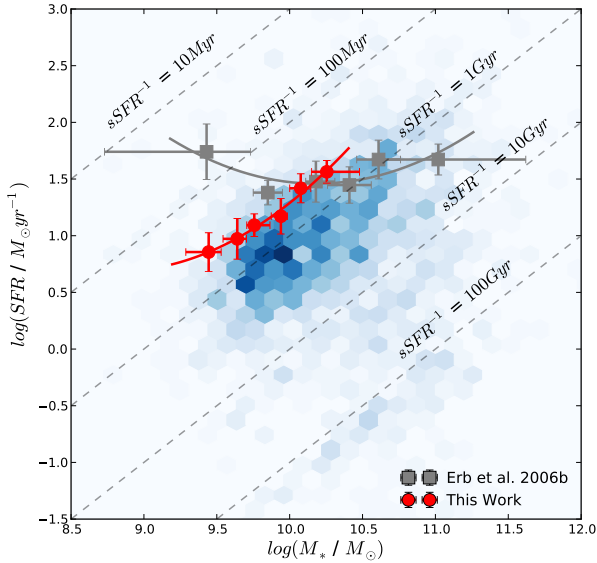


**Figure 7.** The  $M_*$ -SFR plane. Red circles represent SFRs for the stacked galaxies presented in this paper with SFR measured from the  $H\beta$  flux of the stacked spectra, converted to  $H\alpha$  via the common conversion factor  $H\alpha/H\beta = 2.86$  (Kennicutt 1998). The grey squares represent SFRs for the stacked galaxies from Erb et al. (2006b) (grey squares) with SFR measured directly from  $H\alpha$ . The points are overlaid on a 2D histogram (in blue) of  $\sim 3000$  galaxies at  $2 < z < 2.5$  from Whitaker et al. (2012) to provide a visual reference for the region of the  $M_*$ -SFR plane we are sampling. Below  $\log(M / M_\odot) < 10.0$  the galaxies presented in this paper probe lower median values of SFR at a given stellar mass than Erb et al. (2006b). This implies, assuming the FMR, that in these mass bins we should measure higher metallicities. Polynomial fits to the Erb et al. (2006b) data (grey line) and the data presented here (red line) are indicated on the plot, these lines represent two slices along the FMR surface. The predicted positions of galaxies in the MZ plane (Fig. 6) are derived from these polynomial fits.

for each galaxy stack. Again it can be seen that the Erb et al. (2006b) data are consistent with the FMR whilst the galaxies presented in this paper lie offset by  $\sim 0.3$  dex (dashed red line). Also shown in Fig. 8 is the  $\sim 0.5$  dex offset of the AMAZE/LSD galaxies (Maiolino et al. 2008; Mannucci et al. 2009) at  $z \sim 3$ . The offset was calculated by taking the median values of mass, metallicity, and SFR of the individual galaxies quoted in those papers. We convert the stellar mass from Maiolino et al. (2008) to be consistent with the Chabrier IMF used in this analysis.

This offset of the  $z \sim 3$  galaxies was also noted in Mannucci et al. (2010). As discussed in Section 2.3.3 we use the same calibration and the same set of emission lines to measure metallicities as the AMAZE/LSD surveys. Furthermore, our method of metallicity measurement is shown to return consistent results (see Fig. 4). On the other hand, one difference between our analysis and that of Erb et al. (2006b) is the metallicity indicator used.

We note that stacking in bins of mass is diluting the SFR information and may introduce trends depending on how each bin is populated in terms of SFR, since metallicity

is also SFR dependent. However we choose to stack in bins of stellar mass in this paper for a direct comparison with Erb et al. (2006b). We have tested stacking in a grid of stellar mass and SFR (following Mannucci et al. (2010)) by splitting the sample evenly into three stellar mass bins and splitting each bin into two bins of SFR, using this method we observe an FMR offset consistent with the one presented in Fig. 8. We also observe a consistency with the form of the FMR in that, in a given mass bin, the stack with lower metallicity has a higher measured SFR.

The fact that the  $z \sim 2$  galaxies presented here are offset from the FMR, as are the  $z \sim 3$  galaxies, whilst the  $z \sim 2$  galaxies of Erb et al. (2006b) are in agreement, suggests that the choice of metallicity indicator may be affecting the measured metallicities. At first sight it appears that this should not be the case, since all line ratios are calibrated to the same metallicity scale. However, these calibrations were made in the local Universe and the galaxies used to derive the calibrations may not be representative of typical high-redshift galaxies. Below we investigate whether a change in the ionization conditions of HII regions at high redshifts affects the consistency of metallicity measurements using different sets of line ratios.

### 3.3 Photoionization Conditions

The metallicity calibrations outlined in Maiolino et al. (2008) are calibrated against local star-forming galaxies. The line flux ratios used in these calibrations are known to have other dependencies (e.g. ionization parameter, gas density) and therefore to use them at high redshift we have to assume the conditions in star-forming galaxies at high redshift do not differ significantly from those at low redshift. However it is known that many properties of galaxies change at high redshift; for example at  $z \sim 2$  galaxies are on average more compact and have higher SFR (e.g. Buitrago et al. 2008; McLure et al. 2013; Whitaker et al. 2012). These changes may affect the physical conditions within these galaxies. One probe of the physical conditions of HII regions in galaxies is the BPT diagram.

#### 3.3.1 BPT diagram

The most commonly used diagnostic of photoionization conditions in HII regions is the BPT diagram (Baldwin, Phillips, & Terlevich 1981) which has traditionally been used to separate star-forming galaxies from AGN in local galaxies. In recent years there have been indications that the ionization conditions of HII regions at  $z > 1$  are different from those in the local Universe (e.g. Shapley et al. 2005; Erb et al. 2006a; Liu et al. 2008; Hainline et al. 2009; Nakajima et al. 2013). The BPT diagram is shown in Fig. 9. Plotted in black are a sample of galaxies from the SDSS DR7 MPA-JHU data release (Brinchmann et al. 2013) in the redshift range  $0.04 < z < 0.5$ . Fig. 9 also shows a handful of galaxies at  $z \sim 2$  which have  $[OIII]\lambda 5007$ ,  $H\beta$ ,  $H\alpha$  and  $[NII]$  measurements and can therefore be placed on the BPT diagram (Hainline et al. 2009; Belli et al. 2013; Newman et al. 2013). It is evident that  $z \sim 2$  galaxies are offset from the local BPT relation for star-forming galaxies, particularly striking are the large values of the  $[OIII]\lambda 5007/H\beta$  ratio seen at these



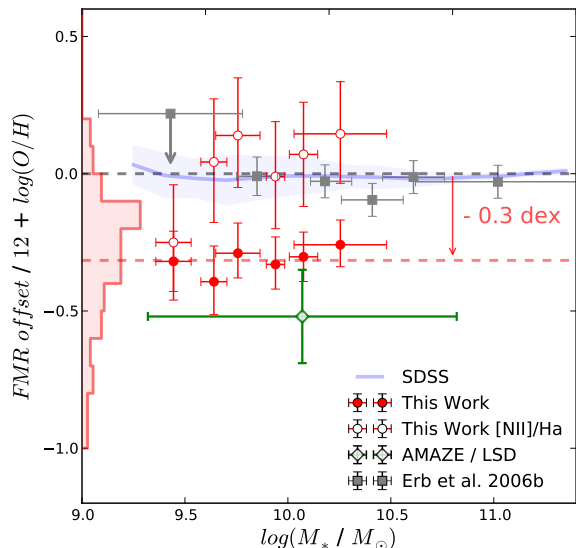


**Figure 8.** The difference in the observed values of metallicity from those predicted by the FMR as a function of stellar mass for various samples. The blue line is the original SDSS sample of Mannucci et al. (2010) with the blue shaded region representing the  $1\sigma$  dispersion. The average dispersion of the sample is 0.05 dex. The filled red circles represent the galaxies presented in this paper with metallicities measured from the  $[\text{OII}]\lambda 3727$ ,  $[\text{OIII}]\lambda 4958,5007$  and  $\text{H}\beta$  nebular emission lines. The green diamond is a combination of  $z \sim 3$  galaxies from the AMAZE/LSD surveys (Maiolino et al. 2008; Mannucci et al. 2009) with metallicities measured in the same way. The grey squares are the Erb et al. (2006b) galaxies with metallicities derived from  $[\text{NII}]$  and  $\text{H}\alpha$ . The predicted value of  $12 + \log(\text{O}/\text{H})$  is derived from the FMR equation of Mannucci et al. (2010) using the measured values of mass and SFR. Our results, within the error bars, are not consistent with the same FMR derived in the local Universe persisting out to  $z \sim 2$ , and yield a median offset of  $\sim 0.3$  dex. The AMAZE/LSD  $z \sim 3$  galaxies are also inconsistent with the FMR. The Erb et al. (2006b) data is consistent with the FMR derived in the local Universe. As argued in Section 3.3 the data presented here can be brought into agreement with the FMR if the we infer a  $[\text{NII}]/\text{H}\alpha$  line ratio from the BPT diagram using the  $[\text{OIII}]\lambda 4958,5007/\text{H}\beta$  to  $[\text{NII}]/\text{H}\alpha$  conversions of Kewley et al. (2013a). The open red circles show the FMR offset for the metallicities derived from these theoretical  $[\text{NII}]/\text{H}\alpha$  ratios.

redshifts, clearly offset from the locus of the SDSS galaxies. The offset is also seen at lower redshifts, for example in the DEEP2 survey of  $1 < z < 1.5$  star-forming galaxies of Shapley et al. (2005) and the Trump et al. (2013) study of  $z \sim 1.5$  galaxies using MOSFIRE and 3D-HST. For our sample, since we can only measure the  $[\text{OIII}]\lambda 5007/\text{H}\beta$  ratio, we show a histogram of the values for our full galaxy sample on the y axis of Fig. 9. Our results are consistent with previously measured  $z \sim 2$  ratios of individual objects, the median  $[\text{OIII}]\lambda 4958,5007/\text{H}\beta$  ratio of our sample is 0.63. Of course, elevated values of the  $[\text{OIII}]\lambda 5007/\text{H}\beta$  ratio are not necessarily an indication of change in ionization conditions in HII regions as the ratio is also strongly metallicity dependent.

However, Brinchmann et al. (2008) and Kewley et al.

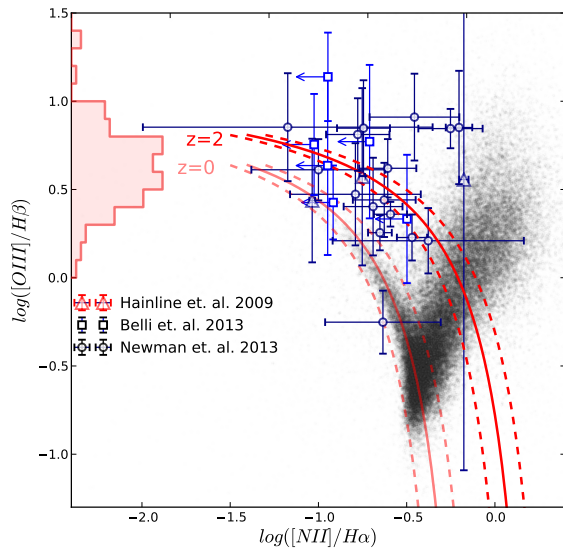


**Figure 9.** The BPT diagram of  $\log([\text{NII}]/\text{H}\alpha)$  vs.  $\log([\text{OIII}]/\text{H}\beta)$  used for diagnosing HII regions via emission-line ratios. The grey points show a sample of local SDSS galaxies from Brinchmann et al. (2013). The blue data points with error bars show the current data for  $z \sim 2$  galaxies with measurements in all four emission lines, the open triangles are three galaxies from Hainline et al. (2009), the open squares are a sample of gravitationally lensed galaxies from Belli et al. (2013) and the open circles are from Newman et al. (2013). A histogram of the distribution of the  $[\text{OIII}]\lambda 5007/\text{H}\beta$  ratio of the individual galaxies in this paper is shown on the y axis; the observed ratios are consistent with the other  $z \sim 2$  data. The two red lines show the ridge line of normal star-forming galaxies on the BPT diagram at  $z = 0$  and  $z = 2$  respectively, taken from the theoretical calibration of Kewley et al. (2013a). The  $z = 2$  offset is attributed to a evolution in the ionization condition in HII regions at high redshift causing a change in the ionization parameter (Brinchmann et al. 2008; Kewley et al. 2013a). As argued in the text, since the metallicity calibrations of Maiolino et al. (2008) are based on local SDSS galaxies falling on the  $z = 0$  sequence, any offset from this ridge line at high redshift will lead to a discrepancies between metallicities derived from the  $[\text{OIII}]\lambda 5007/\text{H}\beta$  and  $[\text{NII}]/\text{H}\alpha$  ratios.

(2013a,b) have investigated the evolution of the star-forming sequence with redshift and claim that a larger ionization parameter, higher electron density and harder ionizing radiation field may be the cause of this evolution. Trump et al. (2013) on the other hand claim to detect nuclear activity in 2/3 of a sample of  $z \sim 1.5$  galaxies, arguing that the majority of high-redshift galaxies show evidence for nuclear activity, such that high-redshift galaxies are offset from the star-forming line in the BPT diagram in the same way AGN are offset in local galaxies. However it is not clear that AGN diagnostics for local Universe galaxies can be directly applied to galaxies at high redshift given a change in ionization conditions (Kewley et al. 2013b). Most recently Kewley et al. (2013a) used cosmological hydrodynamical simulations to investigate how the positions of star-forming galaxies on the BPT diagram evolve given different sets of assumptions for the ionization conditions within galaxies, concluding that the position changes depending on the hardness of ionizing

radiation field, ionization parameter, and electron densities. Kewley et al. (2013a) provide a redshift dependent equation giving the position for the star-forming sequence of galaxies on the BPT diagram, the position of this main sequence at  $z = 0$  and  $z = 2$  is shown in Fig. 9. These star-forming sequences can be seen to be consistent with both the SDSS and current  $z \sim 2$  data.

If our data are consistent with an elevated ionization parameter this suggests our galaxies would also lie offset from the  $z=0$  star-forming galaxy sequence, and on the  $z=2$  star-forming sequence as shown in Fig. 9.

### 3.3.2 $O32$ vs. $R_{23}$ diagram

We can investigate the ionization state of our  $z \sim 2$  galaxies directly using the  $O32$  vs.  $R_{23}$  diagram (Lilly et al. 2003). The  $[OIII]\lambda 4958,5007/[OII]\lambda 3727$  ratio ( $O32$ ) is ionization-parameter sensitive (Kewley & Dopita 2002; Brinchmann et al. 2008) and we can use this to test the typical ionization conditions in our galaxy sample. However,  $O32$  is also sensitive to metallicity (Nagao et al. 2006), so a second more metallicity sensitive ratio must be used to break the degeneracy. We follow the method employed in various studies in the literature by plotting  $O32$  vs  $R_{23}$  (e.g. Lilly et al. 2003; Hainline et al. 2009; Nakajima et al. 2013). The comparison is shown in Fig. 10 where we again plot the SDSS sample plus a sample at intermediate redshift ( $0.47 < z < 0.92$ ) from Lilly et al. (2003). Our data seem to support the conclusions of Hainline et al. (2009) and Nakajima et al. (2013) that galaxies at  $z > 2$  are systematically offset toward larger values of  $O32$  at a given value of  $R_{23}$ . As discussed by those authors this is evidence for higher ionization parameters at fixed metallicity, and so our data are consistent with a higher ionization parameter as seen in other  $z \sim 2$  galaxies.

### 3.3.3 Implications for metallicity measurements

An offset in the position of star-forming galaxies in the BPT diagram has implications for the metallicities derived from either the oxygen and  $H\beta$  or  $[NII]$  and  $H\alpha$  emission-line ratios. Since the metallicity calibrations of Maiolino et al. (2008) were made using local star-forming galaxies, metallicities derived from either oxygen and  $H\beta$  lines, or  $[NII]/H\alpha$ , will only be consistent for galaxies which lie on the  $z = 0$  star-forming sequence. Fig. 11 illustrates this by comparing the  $[NII]/H\alpha$  ratios inferred in three different ways for the individual galaxies in our sample. Firstly, we use the measured metallicities from oxygen and  $H\beta$  lines and work backwards from the Maiolino et al. (2008) calibrations to infer a  $[NII]/H\alpha$  ratio via:

$$\log([NII]/H\alpha) = -0.7732 + 1.2357x - 0.2811x^2 - 0.7201x^3 - 0.3330x^4 \quad (3)$$

Where  $x = 12 + \log(O/H) - 8.69$ .

Secondly and thirdly, we take the measured values of the  $[OIII]\lambda 5007/H\beta$  ratio and use the BPT star-forming sequence of Kewley et al. (2013a) at  $z \sim 2$  and  $z = 0$  respectively to infer a  $[NII]/H\alpha$  ratio via:

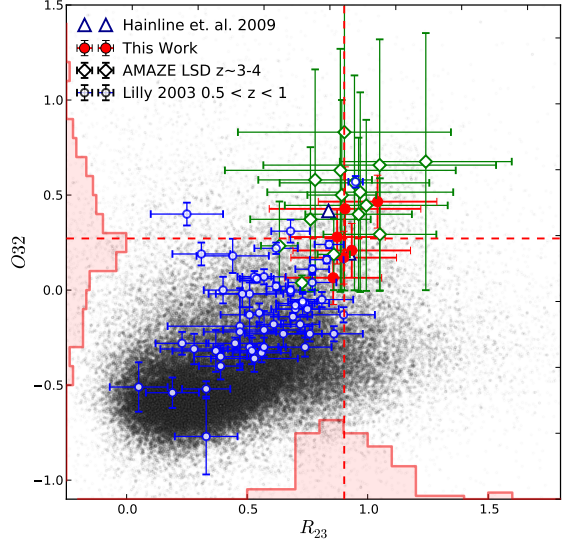


**Figure 10.** The  $O32$  vs  $R_{23}$  diagnostic diagram used to differentiate change in ionization conditions from a change in metallicity of galaxies (Lilly et al. 2003; Hainline et al. 2009; Nakajima et al. 2013). The stacked galaxies in our sample are represented by filled red circles and the distribution of the individual galaxies are shown as histograms on each axis. The open blue circles represent a sample of  $0.5 < z < 1$  galaxies taken from Lilly et al. (2003), the open green diamonds are the AMAZE/LSD sample of  $z \sim 3-4$  galaxies from Maiolino et al. (2008) and Mannucci et al. (2009). The galaxies in our sample are consistent with a systematic offset to higher values of  $O32$  at a fixed  $R_{23}$ , indicative of an increased ionization parameter.

$$\log([NII]/H\alpha) = 0.1833z - 0.08 + \frac{0.61}{\log([OIII]/H\beta) - 1.1 - 0.03z}. \quad (4)$$

It can be seen from Fig. 11 that assuming the Maiolino et al. (2008) calibrations leads to systematically lower predicted values of the  $[NII]/H\alpha$  ratio compared to those derived using Kewley et al. (2013a) at  $z \sim 2$ . By contrast the Maiolino et al. (2008) calibrations are in good agreement with  $[NII]/H\alpha$  ratios derived using Kewley et al. (2013a) at  $z = 0$ . This implies the Maiolino et al. (2008) calibrations are not applicable to high-redshift galaxies since, given a metallicity measured from the oxygen and  $H\beta$  lines, they predict  $[NII]/H\alpha$  ratios consistent with the local star-forming galaxy sequence, whereas  $z \sim 2$  galaxies lie offset from this sequence towards higher  $[NII]/H\alpha$  ratios.

The effect of using the Kewley et al. (2013a) calibration on the FMR is shown in Fig. 8 where the open red circles represent the metallicities derived from the  $[NII]/H\alpha$  ratio assuming the Kewley et al. (2013a) conversion at the median redshift of the stacks ( $z \sim 2$ ). These theoretical  $[NII]/H\alpha$  ratios return systematically higher metallicities than those derived from oxygen and  $H\beta$  lines. This suggests metallicities at high redshift based on the oxygen and  $H\beta$  lines are not directly comparable to metallicities measured from the  $[NII]/H\alpha$  ratio. It can also be seen from Fig. 8 that these the-

oretical  $[\text{NII}]/\text{H}\alpha$  metallicities are in better agreement with the FMR. Thus the consistency of the Erb et al. (2006b) data with the FMR, and the inconsistency of our data with it, can be explained by this evolution of galaxies in the BPT diagram with redshift.

### 3.3.4 Comparison with Newman et al. (2013) data

To further investigate the discrepancy between line indicators we took a sample of eleven  $z \sim 2$  galaxies from Newman et al. (2013) which have flux measurements in the  $[\text{NII}]$ ,  $\text{H}\alpha$ ,  $[\text{OIII}]\lambda 5007$  and  $\text{H}\beta$  lines and have measured masses and SFRs. The masses were derived using a Chabrier (2003) IMF so no conversion was necessary for comparison with our results. Metallicities were derived from the  $[\text{NII}]/\text{H}\alpha$  and  $[\text{OIII}]\lambda 5007/\text{H}\beta$  line ratios individually and the offset from the predicted FMR value computed as described in Sec. 3.2.

Note that the full set of oxygen and  $\text{H}\beta$  calibrations used on our data could not be used on the Newman et al. (2013) data so oxygen and  $\text{H}\beta$  metallicities were derived from the  $[\text{OIII}]\lambda 5007/\text{H}\beta$  ratio alone. When used independently the  $[\text{OIII}]\lambda 5007/\text{H}\beta$  metallicity calibration is double-valued (see Maiolino et al. 2008), so to derive a metallicity from the  $[\text{OIII}]\lambda 4958, 5007/\text{H}\beta$  ratio solely it is necessary to choose between the upper and lower solutions. For each galaxy in the Newman et al. (2013) sample the upper solution was taken, as it was in agreement with the high metallicities implied from the  $[\text{NII}]/\text{H}\alpha$  solution. Nevertheless, even when taking the upper solution for  $[\text{OIII}]\lambda 5007/\text{H}\beta$ , the  $[\text{NII}]/\text{H}\alpha$  ratio returns systematically higher values of metallicity in better agreement with the FMR. This is illustrated in Fig. 12. The median and MAD for the  $[\text{NII}]/\text{H}\alpha$  ratio and  $[\text{OIII}]\lambda 5007/\text{H}\beta$  ratio respectively are  $-0.10 \pm 0.09$  dex and  $-0.41 \pm 0.41$  dex. It is also interesting to note that the Newman et al. (2013) data probe a higher-mass regime, similar to the Erb et al. (2006b) sample, indicating this effect is seen across a wide range in mass  $\sim 9.5 < \log(M/M_\odot) < 11.5$ . Thus it seems that the higher  $[\text{NII}]/\text{H}\alpha$  derived metallicities, implied for our sample from Kewley et al. (2013a), are also observed in this small sample  $z \sim 2$  galaxies.

To summarize these arguments suggest that if spectra are obtained in the K band for our galaxy sample such that the  $[\text{NII}]/\text{H}\alpha$  ratio can be measured, this ratio will return a higher metallicities by  $\sim 0.3 - 0.5$  dex over metallicities derived from the oxygen and  $\text{H}\beta$  line using the Maiolino et al. (2008) metallicity calibrations. Thus from the  $[\text{NII}]/\text{H}\alpha$  ratio one will observe better consistency with the FMR as in Erb et al. (2006b), whilst from the oxygen and  $\text{H}\beta$  lines an offset will be observed as in this work and at  $z \sim 3$  (Maiolino et al. 2008; Mannucci et al. 2009). A detailed comparison of the two line ratios as metallicity indicators is beyond the scope of the present work, though resolving this issue is clearly of key importance if we want to conclude anything more definitive regarding the FMR at high redshift. Our results and other evidence from the literature (e.g. Ly et al. 2013; Nakajima & Ouchi 2013) suggest current metallicity calibrations need to be revised to take into account the high ionization parameters observed at high redshift.

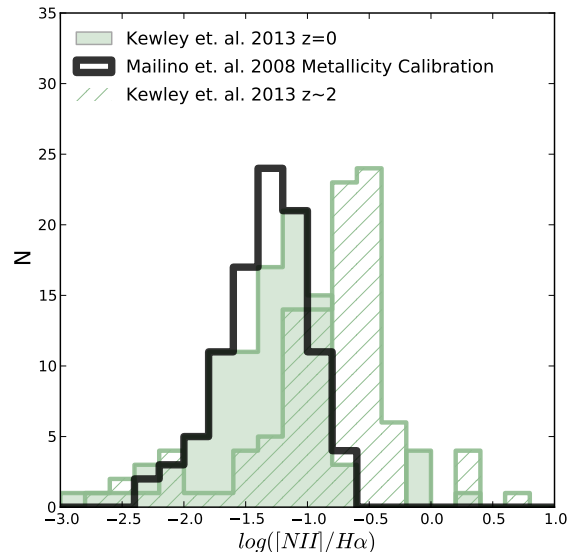


**Figure 11.** Histograms showing the inferred  $[\text{NII}]/\text{H}\alpha$  ratios for the individual galaxies in our sample. The open black histogram is the  $[\text{NII}]/\text{H}\alpha$  ratio derived using the measured metallicity with the Maiolino et al. (2008) metallicity calibrations (Eq. 3). The filled green histogram is the ratio derived from the measured  $[\text{OIII}]\lambda 5007/\text{H}\beta$  ratio and using the BPT diagram star-forming galaxy main sequence equation at  $z=0$  from Kewley et al. (2013a) (Eq. 4). These two histograms are in good agreement which is as expected since the Maiolino et al. (2008) calibrations were made using local Universe galaxies. The median and median absolute deviation (MAD) of the ratios derived from Maiolino et al. (2008) and Kewley et al. (2013a) ( $z = 0$ ) respectively are  $-1.34 \pm 0.2$  dex and  $-1.26 \pm 0.3$  dex. The hatched green histogram is derived in the same way as the filled green histogram except using the galaxies redshift in Eq. 4 ( $z \sim 2$ ). The median and MAD of this distribution is  $-0.74 \pm 0.3$  dex. Assuming star-forming galaxies evolve across the BPT diagram with redshift leads to higher predicted values of  $[\text{NII}]/\text{H}\alpha$  which are incompatible with the metallicity calibrations of Maiolino et al. (2008). This implies metallicities measured at  $z \sim 2$  using  $[\text{NII}]/\text{H}\alpha$  will be higher than those using oxygen and  $\text{H}\beta$  lines.

## 4 SUMMARY AND CONCLUSIONS

We have selected a sample of 103 galaxies in the redshift range  $2.0 < z < 2.3$  from an independent reduction of the 3D-HST spectroscopic grism survey. In this redshift range the  $[\text{OII}]\lambda 3727$ ,  $[\text{OIII}]\lambda 4958, 5007$  and  $\text{H}\beta$  emission lines fall within the wavelength range of the grism spectra. Our aim is to use those emission lines to measure the metallicities of galaxies and measure their masses from the ancillary CANDELS photometry available in the 3D-HST survey fields. We stack the galaxies in bins of stellar mass and construct a mass-metallicity relationship for this sample, which we can directly compare with the previous  $z \sim 2$  study of Erb et al. (2006b). We then measure the SFR from the  $\text{H}\beta$  line and use this to investigate the FMR at these redshifts. Below is a summary of our results.

- We measure the metallicities of our galaxies from the  $[\text{OII}]\lambda 3727$ ,  $\text{H}\beta$  and  $[\text{OIII}]\lambda 4958, 5007$  emission lines via the

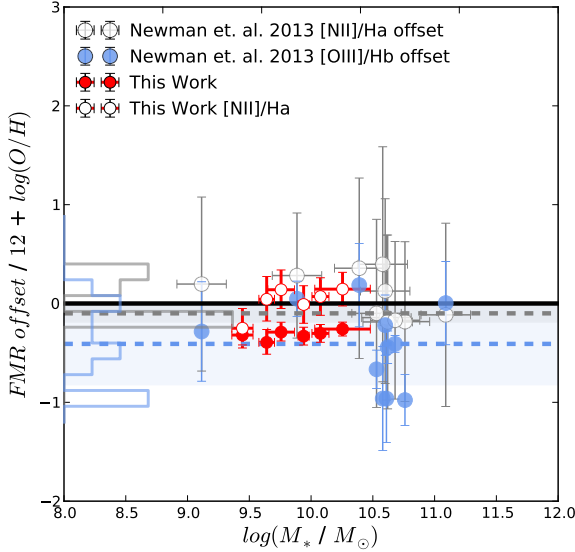


**Figure 12.** The FMR offset for a sample of  $z \sim 2$  star-forming galaxies taken from Newman et al. (2013). This galaxy sample has measurements for both the  $[\text{NII}]/\text{H}\alpha$  ratio and  $[\text{OIII}]\lambda 5007/\text{H}\beta$  ratios. We can therefore measure the metallicities from these ratios individually using the Maiolino et al. (2008) calibrations and clarify observationally the theoretical arguments made in Sec. 3.3.3. Open grey circles show the metallicities derived from the  $[\text{NII}]/\text{H}\alpha$  ratio and the filled blue circles show the metallicities derived from the  $[\text{OIII}]\lambda 4958, 5007/\text{H}\beta$  ratio. On the y axis the grey and blue histograms show the distribution of the individual points with the horizontal dashed lines representing the median values of the distributions. It can be seen that the  $[\text{NII}]/\text{H}\alpha$  ratio returns systematically higher metallicities in better agreement with the FMR. This is in agreement with what is found for the galaxies in our sample when a  $[\text{NII}]/\text{H}\alpha$  ratio is derived from the Kewley et al. (2013a) calibration. The median and MAD for the  $[\text{NII}]/\text{H}\alpha$  ratio and  $[\text{OIII}]\lambda 5007/\text{H}\beta$  ratio respectively are  $-0.10 \pm 0.09$  dex and  $-0.41 \pm 0.41$  dex., the MAD is shown by the shaded region around the median line. For reference the galaxies presented in this paper are plotted as filled red and open red circles as in Fig. 8.

calibrations of Maiolino et al. (2008). We find a MZR in our galaxy sample consistent with the MZR reported elsewhere in the literature (e.g. Erb et al. 2006b; Mannucci et al. 2009; Yuan et al. 2013). We observe a decrease in metallicity with a decrease in mass of our galaxy stacks (Fig. 6). However our MZR is offset to lower metallicities at a given stellar mass from the  $z \sim 2$  MZR of Erb et al. (2006b).

- We investigate this metallicity offset using the FMR proposed by Mannucci et al. (2010) which incorporates mass, metallicity and SFR in an attempt to explain the scatter and evolution of the MZR. However we find our data are apparently inconsistent with the FMR. We measure metallicities lower by  $\sim 0.3$  dex from those predicted from the FMR given our measured masses and SFRs (Fig. 8). The previous  $z \sim 2$  data of Erb et al. (2006b) are consistent with the FMR as discussed in Mannucci et al. (2010), therefore there is a discrepancy between the current  $z \sim 2$  data. One difference between the Erb et al. (2006b) study and our own

is the metallicity indicator used. Erb et al. (2006b) use the  $[\text{NII}]/\text{H}\alpha$  ratio whereas our metallicities are based on the oxygen and  $\text{H}\beta$  lines. Interestingly our method for metallicity measurement follows the previous  $z \sim 3$  MZR studies (Maiolino et al. 2008; Mannucci et al. 2009) who find a similar offset from the FMR using the same set of emission lines.

- We investigate the ionization conditions of our galaxies to attempt to explain the FMR offset. We construct a O32 vs  $R_{23}$  diagram following the method of Lilly et al. (2003), Hainline et al. (2009) and Nakajima et al. (2013) (Fig 10). We find, consistent with previous  $z \sim 2$  data, evidence for an enhancement of the O32 ratio at fixed value of  $R_{23}$  indicative of an enhanced ionization parameter in these galaxies at fixed metallicity.

- We note that from small samples of  $z \sim 2$  star-forming galaxies with  $[\text{OII}]\lambda 3727$ ,  $\text{H}\beta$ ,  $[\text{OIII}]\lambda 4958, 5007$ ,  $[\text{NII}]$  and  $\text{H}\alpha$  measured (e.g. Hainline et al. 2009; Belli et al. 2013; Newman et al. 2013), there is evidence that higher ionization parameters cause an offset from the star-forming galaxy sequence in the BPT diagram of local galaxies (Fig. 9). This offset has recently been quantified by Kewley et al. (2013a) who provide an equation for the evolution of the star-forming sequence with redshift (Fig. 9 and Eq. 4). Given the evidence for an increased ionization parameter in our galaxies, and  $[\text{OIII}]\lambda 5007/\text{H}\beta$  ratios consistent with other  $z \sim 2$  samples, we conclude our galaxies would most likely also lie offset from the  $z=0$  star-forming galaxy sequence.

- Working backwards from our metallicity measurements we can infer the expected  $[\text{NII}]/\text{H}\alpha$  ratio of our galaxies from the Maiolino et al. (2008) calibrations (Eq. 3). We can also infer the expected  $[\text{NII}]/\text{H}\alpha$  ratio from the Kewley et al. (2013a) BPT main sequence calibration at  $z \sim 2$  and  $z = 0$  (Eq. 4). The inferred ratios from the Maiolino et al. (2008) calibrations are systematically lower than the inferred ratios from Kewley et al. (2013a) at  $z \sim 2$  but consistent with those at  $z = 0$  (Fig. 11). This implies the  $[\text{OIII}]\lambda 5007/\text{H}\beta$  and  $[\text{NII}]/\text{H}\alpha$  metallicity calibrations are not comparable for galaxies significantly offset from the star-forming main sequence of the BPT diagram, such as the currently observed galaxies high redshift.

- Taking the inferred  $[\text{NII}]/\text{H}\alpha$  ratios from the Kewley et al. (2013a) calibration at  $z \sim 2$  we find our galaxies would fall into better agreement with the FMR (Fig. 8). For further investigation we also take a sample of 11  $z \sim 2$  galaxies with measured  $[\text{NII}]$ ,  $\text{H}\alpha$ ,  $[\text{OIII}]\lambda 5007$  and  $\text{H}\beta$  fluxes from Newman et al. (2013) and confirm that the metallicities derived using the Maiolino et al. (2008) calibrations are systematically higher than when using the  $[\text{NII}]/\text{H}\alpha$  ratio (Fig. 12), following the trend in our data inferred using Kewley et al. (2013a). This further supports the conclusion that metallicities derived from the oxygen and  $\text{H}\beta$  lines are not equivalent to those derived using  $[\text{NII}]/\text{H}\alpha$  at high redshift.

- We conclude a major cause of the discrepancy between our data and the FMR, as well as the  $z \sim 3$  data of Maiolino et al. (2008) and Mannucci et al. (2009) is the result of using locally calibrated metallicity relations. The evolution of the FMR at high redshift cannot be quantified until we have metallicity calibrations accounting for the change in physical conditions of star-forming regions at these redshifts.



## 5 ACKNOWLEDGMENTS

FC and MC acknowledge the support of the Science and Technology Facilities Council (STFC) via the award of an STFC Studentship and an STFC Advanced Fellowship, respectively. RJM acknowledges the support of the European Research Council via the award of a Consolidator Grant (PI McLure). JSD acknowledges the support of the European Research Council via the award of an Advanced Grant, and the support of the Royal Society via a Wolfson Research Merit Award. This work is based on observations taken with the NASA/ESA HST, which is operated by the Association of Universities for Research in Astronomy, Inc., under NASA contract NAS5-26555. This work is based (in part) on observations made with the Spitzer Space Telescope, which is operated by the Jet Propulsion Laboratory, California Institute of Technology under a contract with NASA. This research made use of Astropy, a community-developed core Python package for Astronomy (Collaboration et al. 2013), NumPy and SciPy (Oliphant 2007), Matplotlib (Hunter 2007), IPython (Pérez & Granger 2007) and NASA's Astrophysics Data System Bibliographic Services.

## References

- Baldwin J. A., Phillips M. M., Terlevich R., 1981, *PASP*, 93, 5
- Belli S., Jones T., Ellis R. S., Richard J., 2013, *ApJ*, 772, 141
- Bowler R. A. A. et al., 2012, *MNRAS*, 426, 2772
- Brammer G. B., van Dokkum P. G., Coppi P., 2008, *ApJ*, 686, 1503
- Brammer G. B. et al., 2012, *ApJS*, 200, 13
- Brinchmann J., Charlot S., Kauffmann G., Heckman T., White S. D. M., Tremonti C., 2013, *MNRAS*, 432, 2112
- Brinchmann J., Pettini M., Charlot S., 2008, *MNRAS*, 385, 769
- Bruzual G., Charlot S., 2003, *MNRAS*, 344, 1000
- Buitrago F., Trujillo I., Conselice C. J., Bouwens R. J., Dickinson M., Yan H., 2008, *ApJ*, 687, L61
- Calzetti D., Armus L., Bohlin R. C., Kinney A. L., Koornneef J., Storch-Bergmann T., 2000, *ApJ*, 533, 682
- Chabrier G., 2003, *PASP*, 115, 763
- Civano F. et al., 2012, *ApJS*, 201, 30
- Collaboration T. A. et al., 2013, *ArXiv e-prints*
- Cowie L. L., Barger A. J., 2008, *ApJ*, 686, 72
- Cresci G., Mannucci F., Sommariva V., Maiolino R., Marconi A., Brusa M., 2012, *MNRAS*, 421, no
- Erb D. K., Shapley A. E., Pettini M., Steidel C. C., Reddy N. A., Adelberger K. L., 2006b, *ApJ*, 644, 813
- Erb D. K., Steidel C. C., Shapley A. E., Pettini M., Reddy N. A., Adelberger K. L., 2006a, *ApJ*, 647, 128
- Förster Schreiber N. M. et al., 2009, *ApJ*, 706, 1364
- Galametz A. et al., 2013, *ApJS*, 206, 10
- Grogin N. A. et al., 2011, *ApJS*, 197, 35
- Guo Y. et al., 2013, *ApJS*, 207, 24
- Hainline K. N., Shapley A. E., Kornei K. A., Pettini M., Buckley-Geer E., Allam S. S., Tucker D. L., 2009, *ApJ*, 701, 52
- Hunter J. D., 2007, *Computing In Science & Engineering*, 9, 90
- Ilbert O. et al., 2006, *A&A*, 457, 841
- Kauffmann G. et al., 2003, *MNRAS*, 346, 1055
- Kennicutt R. C. J., 1998, *A&ARv*, 36, 189
- Kewley L. J., Dopita M. A., 2002, *ApJS*, 142, 35
- Kewley L. J., Dopita M. A., Leitherer C., Davé R., Yuan T., Allen M., Groves B., Sutherland R., 2013a, *ApJ*, 774, 100
- Kewley L. J., Ellison S. L., 2008a, *ApJ*, 681, 1183
- Kewley L. J., Ellison S. L., 2008b, *ApJ*, 681, 1183
- Kewley L. J., Maier C., Yabe K., Ohta K., Akiyama M., Dopita M. A., Yuan T., 2013b, *ApJ*, 774, L10
- Koekemoer A. M. et al., 2011, *ApJS*, 197, 36
- Kümmel M., Walsh J. R., Pirzkal N., Kuntschner H., Pasquali A., 2009, *PASP*, 121, 59
- Lara-Lopez M. A. et al., 2010, *A&A*, 521, L53
- Lara-López M. A., López-Sánchez Á. R., Hopkins A. M., 2013, *ApJ*, 764, 178
- Lilly S. J., Carollo C. M., Stockton A. N., 2003, *ApJ*, 597, 730
- Liu X., Shapley A. E., Coil A. L., Brinchmann J., Ma C.-P., 2008, *ApJ*, 678, 758
- Ly C., Malkan M. A., Nagao T., Kashikawa N., Shimasaku K., Hayashi M., 2013, *ArXiv e-prints*, 7712
- Maiolino R. et al., 2008, *A&A*, 488, 463
- Mannucci F., Cresci G., Maiolino R., Marconi A., Gnerucci A., 2010, *MNRAS*, 408, 2115
- Mannucci F. et al., 2009, *MNRAS*, 398, 1915
- McCracken H. J. et al., 2012, *A&A*, 544, A156
- McLure R. J. et al., 2013, *MNRAS*, 428, 1088
- Mignoli M. et al., 2005, *A&A*, 437, 883
- Nagao T., Maiolino R., Marconi A., 2006, *A&A*, 459, 85
- Nakajima K., Ouchi M., 2013, *eprint arXiv:1309.0207*
- Nakajima K., Ouchi M., Shimasaku K., Hashimoto T., Ono Y., Lee J. C., 2013, *ApJ*, 769, 3
- Newman S. F. et al., 2013, *preprint (arXiv:1306.6676v1)*
- Niino Y., 2012, *ApJ*, 761, 126
- Oliphant T. E., 2007, *Computing in Science & Engineering*, 9, 10
- Panther B., Jimenez R., Heavens A. F., Charlot S., 2008, *MNRAS*, 391, 1117
- Pérez F., Granger B. E., 2007, *Computing in Science & Engineering*, 9, 21
- Pettini M., Pagel B. E. J., 2004, *MNRAS*, 348, L59
- Pirzkal N. et al., 2013, *ApJ*, 772, 48
- Richard J., Jones T., Ellis R., Stark D. P., Livermore R., Swinbank M., 2011, *MNRAS*, 413, 643
- Rodrigues M. et al., 2008, *A&A*, 492, 371
- Roseboom I. G. et al., 2012, *MNRAS*, 426, 1782
- Savaglio S. et al., 2005, *ApJ*, 635, 260
- Shapley A. E., Coil A. L., Ma C.-P., Bundy K., 2005, *ApJ*, 635, 1006
- Storey P. J., Zeppen C. J., 2000, *MNRAS*, 312, 813
- Tremonti C. A. et al., 2004, *ApJ*, 613, 898
- Trump J. R. et al., 2013, *ApJL*, 763, L6
- Whitaker K. E., van Dokkum P. G., Brammer G., Franx M., 2012, *ApJL*, 754, L29
- Xue Y. Q. et al., 2011, *ApJS*, 195, 10
- Yabe K. et al., 2012, *PASJ*, 64, 60
- Yuan T. T., Kewley L. J., Richard J., 2013, *ApJ*, 763, 9
- Zahid H. J., Kewley L. J., Bresolin F., 2011, *ApJ*, 730, 137



This paper has been typeset from a T<sub>E</sub>X/ L<sup>A</sup>T<sub>E</sub>X file prepared  
by the author.